CRYSTAL GROWTH & DESIGN

Article

pubs.acs.org/crystal

# Structure and Thermotropic Phase Behavior of a Homologous Series of *N*-Acylglycines: Neuroactive and Antinociceptive Constituents of Biomembranes

S. Thirupathi Reddy, Krishna Prasad Krovi, and Musti J. Swamy*

School of Chemistry, University of Hyderabad, Hyderabad 500 046, India

Supporting Information

**ABSTRACT:** *N*-Acylglycines (NAGs) with different acyl chains have been found in the mammalian brain and other tissues. They exhibit significant biological and pharmacological properties and appear to play important roles in communication and signaling pathways within and between cells. In view of this, a homologous series of NAGs have been synthesized and characterized in the present study. Differential scanning calorimetric (DSC) studies show that the transition enthalpies and entropies of dry as well as hydrated NAGs exhibit a linear dependence on the acyl chain length. Most of the NAGs show a minor transition below the chain-melting phase transition, suggesting the presence of polymorphism in the solid state. Structures of *N*-myristoylglycine (NMG) and *N*-palmitoylglycine (NPG) were solved in monoclinic system with $C2/c$ and $P2_1$ space groups, respectively. Analysis of the crystal structures show that NAGs are organized in a bilayer fashion, with head-to-head (and tail-to-tail) arrangement of molecules. The acyl chains in both structures are essentially perpendicular to the bilayer plane, which is consistent with a lack of odd−even alternation in the thermodynamic properties. The bilayer is stabilized by strong hydrogen bonding interactions between −COOH groups of the molecules from opposite leaflets as well as N−H···O hydrogen bonds between the amide groups of adjacent molecules in the same leaflet and dispersion interactions among the acyl chains. Powder X-ray diffraction data show that the *d*-spacings for the NAGs with different acyl chains ($n$ = 8−20) exhibit a linear dependence on the chain length, suggesting that all the NAGs investigated here adopt a similar packing arrangement in the crystal lattice. These observations are relevant for understanding the role of *N*-acylglycines in biological membranes.

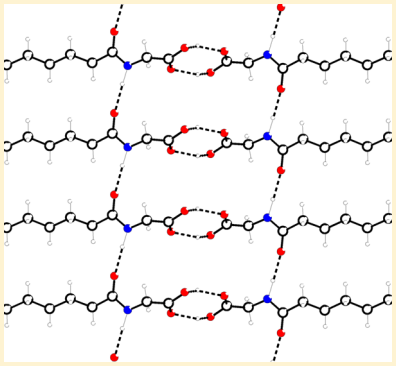

## INTRODUCTION

Conjugates of lipids and amino acids (lipoamino acids) were identified in biological systems over 50 years ago.[1] A family of lipids similar to acyl amino acids containing only one amide bond connecting a fatty acid with ethanolamine, dopamine, or amine has been identified in mammalian tissues.[2−5] Much interest has been generated in such conjugates with the identification of the endocannabinoid *N*-arachidonylethanolamine, also referred to as anandamide, which acts as an endogenous ligand to the cannabinoid receptor CB1, inhibits gap-junction conductance, and reduces the fertilizing capacity of sperm.[6−8] *N*-Arachidonylglycine (NArG), the first lipoamino acid, was synthesized as a structural analog of anandamide with differences of CB1 agonist activity.[9] Huang et al.[10] predicted that NArG would be present in mammalian tissues because it is made up of the naturally occurring compounds glycine and arachidonic acid and demonstrated its presence in bovine and rat brain as well as in other tissues. NArG produces antinociceptive and anti-inflammatory effects, exhibits high-affinity for the orphan GPCR, GPR18, and inhibits the hydrolytic activity of fatty acid amide hydrolase (FAAH) on anandamide as well as glycine transport by GLYT2a.[11−17] It has been reported that NArG is an oxidative metabolite of endogenous cannabinoid anandamide, suggesting that it is a precursor of the former.[18]

Since mammalian tissues also contain saturated fatty acids, it would be expected that corresponding saturated lipoamino acids would be synthesized by the enzymes that conjugate fatty acids and glycine. Indeed, *N*-palmitoylglycine was identified in rat brain and was shown to act as a modulator of calcium influx and nitric oxide production in sensory neurons.[19] Several other NAGs, namely, *N*-stearoylglycine, *N*-oleoylglycine, *N*-linoleoylglycine, and *N*-docosahexaenoylglycine were also found in different parts of the body at different levels, suggesting region-specific functionality.[20] Recent research has shown that besides NAGs, a variety of *N*-acyl amino acids (NAAs) are present in mammalian brain as well as other tissues.[21,22] These and other studies led to considerable interest in investigating the physiological roles and pharmacological potential of *N*-acyl amino acids and neurotransmitters.[5]

While a significant amount of work has been carried out on the biological and pharmacological properties of NAGs, there have been no studies characterizing their physical properties

Received: April 9, 2014
Revised: August 16, 2014
Published: August 22, 2014





dx.doi.org/10.1021/cg500481u | Cryst. Growth Des. 2014, 14, 4944−4954

and interaction with other membrane components. In view of their amphiphilic nature, it would be expected that NAGs with long acyl chains will be incorporated into biomembranes, which in turn may affect their biophysical properties. In order to understand how NAGs interact with lipid membranes and modulate their structure and dynamics, it is imperative to investigate their physical properties and phase behavior, and characterize their interaction with other membrane components such as phospholipids and cholesterol. In view of this, in the present study, we synthesized a homologous series of NAGs ($n$ = 8−20) and investigated their thermotropic phase behavior in dry and hydrated states by DSC, which showed that the transition enthalpy and entropy exhibit a linear dependence on the acyl chain length, without the well-known odd−even alternation observed in other amphiphiles such as long chain carboxylic acids, *N*-acylethanolamines, *N*,*O*-diacylethanolamines and *N*-acyldopamines.[23−26] The lack of odd−even alternation could be explained on the basis of the three-dimensional structure of *N*-myristoylglycine and *N*-palmitoylglycine, which indicated that NAGs form a bilayer structure in the crystal lattice with the acyl chains oriented perpendicular to the bilayer plane.

## EXPERIMENTAL SECTION

**Materials.** Long chain fatty acids ($n$ = 8−20), glycine methyl ester hydrochloride, and lithium hydroxide were purchased from Sigma-Aldrich (Milwaukee, WI, USA). Oxalyl chloride was obtained from Spectrochem (Mumbai, India). Solvents and other chemicals used were of analytical grade and purchased locally. Milli-Q water was used in all experiments.

**Synthesis of *N*-Acylglycines.** NAGs were synthesized by a minor modification of a reported procedure adopted earlier for the synthesis of *N*-hexadecanoylserine (Scheme 1).[27] Briefly, glycine methyl ester hydrochloride (1 mmol) was dissolved in water (4 mL), and sodium bicarbonate (2 mmol) and chloroform (12 mL) were added with vigorous stirring. To this mixture, a chloroform solution of the acid chloride (1 mmol), prepared by the reaction of fatty acid with oxalyl chloride,[28] was added, and the mixture was kept under stirring for 2 h at room temperature. Then the organic phase was washed successively with saturated sodium chloride solution, 0.1 N HCl, and distilled water (twice). The solution was dried over anhydrous sodium sulfate, filtered, and evaporated to dryness under reduced pressure. Recrystallization from hexane at −20 °C yielded *N*-acylglycine methyl ester in 80−85% yield. The methyl ester was converted to the free acid by base-catalyzed hydrolysis for 2 h with lithium hydroxide (10 mmol) in a methanol/water (3:1, v/v) mixture. The pH of the reaction mixture was adjusted to 3.0 by dropwise addition of 2 N HCl, and the NAGs were extracted into ethyl acetate. The extract was then washed with 1 N HCl and twice with distilled water, dried over anhydrous sodium sulfate, filtered, and evaporated to dryness under reduced pressure. Recrystallization from ethyl acetate yielded pure NAGs in about 75−80% yield, which were characterized by melting point, FTIR, and $^1$H and $^{13}$C NMR spectroscopy.

**Scheme 1. Synthesis of *N*-Acylglycines**

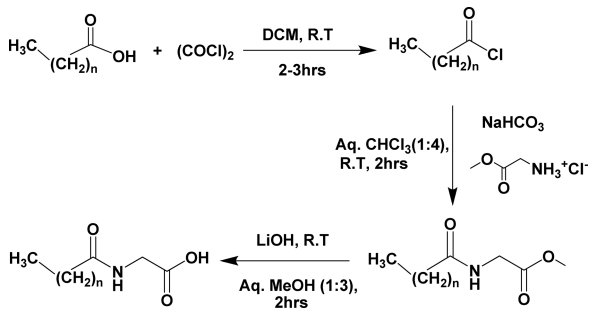


Capillary melting points of NAGs were recorded on a Superfit (Mumbai, India) melting point apparatus.[26] IR spectra (KBr pellet) were recorded on a Jasco FTIR 5300 spectrometer, and $^1$H and $^{13}$C NMR spectra were obtained on a Bruker Avance NMR spectrometer operating at 400 and 100 MHz, respectively. Samples were dissolved in $CDCl_3$ containing a trace of $CD_3OD$ for $^1$H NMR studies, whereas for $^{13}$C NMR spectroscopy, samples were dissolved in $CD_3OD$.

**Differential Scanning Calorimetry.** DSC studies on dry NAGs were carried out on a PerkinElmer PYRIS Diamond differential scanning calorimeter.[26] Heating and cooling scans were performed with 1−2 mg samples taken in aluminum pans from room temperature (~25 °C) to about 140 °C at a scan rate of 1.5°/min. Each sample was subjected to three heating scans and two cooling scans. Transition enthalpies were determined by integrating the area under the transition curve. Transition entropies were calculated from the transition enthalpies according to eq 1, applicable to first order transitions:[29]

$$\Delta H_t = T\Delta S_t \quad (1)$$

where $T$ is the transition temperature and $\Delta H_t$ values were taken at this temperature in order to calculate the corresponding $\Delta S_t$ values.

Hydrated samples for DSC studies were prepared with ca. 4−5 mg of each NAG using the procedure described earlier for *N*-acyldopamines,[26] excepting that in the present study double distilled water was used to hydrate the samples rather than phosphate buffer. DSC studies were carried out on a VP-DSC equipment (MicroCal LLC, Northampton, MA, USA), essentially as described earlier.[26] All samples were subjected to three heating and two cooling scans between 10 and 110 °C at a scan rate of 1°/min. Transition enthalpies were calculated by integrating the area under the transition curve after blank (water) subtraction, normalization, and baseline correction. Transition entropies were determined from the transition enthalpies using eq 1.

**Crystallization, X-ray Diffraction, and Structure Solution.** Colorless, thin plate-type crystals of *N*-myristoylglycine and *N*-palmitoylglycine were grown at room temperature from their solutions in ethyl acetate containing traces of methanol and toluene containing traces of methanol, respectively. X-ray diffraction data were collected at room temperature (ca. 25 °C) on a Bruker SMART APEX CCD area detector system using a graphite monochromator and Mo K$\alpha$ ($\lambda$ = 0.717073 Å) radiation, obtained from a fine-focus sealed tube. The minimum resolution of X-ray diffraction measurements is 0.84 Å. Data reduction was done using the Bruker SAINTPLUS program. Absorption correction was applied using the SADABS program, and refinement was done using the SHELXTL program.[30] Mercury 3.0 and Diamond 2.1 softwares were used for preparing molecular packing and hydrogen bonding diagrams, respectively.

**Powder X-ray Diffraction.** Powder X-ray diffraction patterns of NAGs were recorded on a Bruker SMART D8 Advance powder X-ray diffractometer (Bruker-AXS, Karlsruhe, Germany) using Cu K$\alpha$ radiation ($\lambda$ = 1.5406 Å) at 40 kV and 30 mA. Samples were placed and pressed on a circular rotating disk of the sample holder. The diffracted beam from the sample was detected by a LynxEye PSD data collector. Diffraction patterns were collected for all the NAGs at room temperature over a 2$\theta$ range of 2−50° with a step size of 0.0198°, with a measuring time of 10 s for each step. To investigate polymorphism in NPG, PXRD data were recorded at different temperatures with samples placed in a Anton Paar TTK 450 sample chamber stage with reflection but without movement. An equilibration time of ca. 10 min was given at each temperature before data collection. In these measurements, a 2$\theta$ range of 5−42° with a step size of 0.0198° s$^{-1}$ was used. The appearance of a new polymorph was identified by the appearance of new diffraction peaks. Origin 7 was used for overlaying the experimental PXRD pattern and the simulated PXRD pattern obtained from the single-crystal X-ray diffraction.


dx.doi.org/10.1021/cg500481u | *Cryst. Growth Des.* 2014, 14, 4944−4954

## RESULTS AND DISCUSSION

**Characterization of *N*-Acylglycines.** The homologous series of NAGs ($n$ = 8−20) synthesized in this study have been characterized by FT-IR and $^1$H and $^{13}$C NMR spectroscopy. Representative FTIR and $^1$H NMR spectra of *N*-decanoylglycine are given in Figure S1 and Figure S2, Supporting Information, respectively. IR spectra of all NAGs showed absorption bands corresponding to the amide linkage at 1645−1644 cm$^{-1}$ (amide-I), 1561−1557 cm$^{-1}$ (amide-II), and 3333−3310 cm$^{-1}$ (N−H stretching). Two bands were seen in the carbonyl stretching region, at 1748−1740 and 1707−1700 cm$^{-1}$, which could be due to differences in hydrogen bonding in different polymorphic states. The methylene groups of the acyl chain (and the glycine moiety) show stretching, scissoring and rocking bands at 2922−2849, 1470−1462, and 696−693 cm$^{-1}$, respectively. The values of resonances corresponding to various absorption bands for all the NAGs are given in Table S1, Supporting Information. $^1$H NMR spectra of NAGs showed resonances at 2.15−2.24 $\delta$ (2H, t) and 1.55−1.62 $\delta$ (2H, m) for the methylene groups at $\alpha$ and $\beta$ positions to the amide carbonyl, respectively. Resonances were seen at 3.91−4.22 $\delta$ (2H, s) for the methylene group in the glycine moiety and at 6.16−6.92 $\delta$ (1H, bs) for the amide N−H. Resonance corresponding to the terminal methyl group was seen at 0.80−0.99 $\delta$ (3H, t) whereas resonance for the polymethylene group was observed at 1.17−1.27 $\delta$ (8−32, m). These data for different NAGs are given in Table S2, Supporting Information.

A representative $^{13}$C NMR spectrum of *N*-decanoylglycine is given in Figure S3, Supporting Information. The spectrum shows a resonance at 13.11$\delta$, which corresponds to the methyl group of the acyl chain. Resonances arising from methylene carbons are seen at 22.38, 25.50, 31.70, 35.46, and 40.36 $\delta$ as well as between 28.92 and 29.25 $\delta$ (three peaks with the peak at 29.13 being more intense than the others due to two methylene carbons giving resonances at the same $\delta$ value). Resonances corresponding to the carbonyl moieties of carboxylic acid and amide groups are observed at 171.74 and 175.39 $\delta$, respectively. These values are consistent with the structure of *N*-decanoylglycine. All other NAGs gave similar spectra, except that the intensity of the peak at ∼29.13 $\delta$ increased with increase in the acyl chain length, which can be attributed to several carbon atoms in the middle of the acyl chain having the same chemical shift. $^{13}$C NMR data for all the NAGs are given in Table S3, Supporting Information.

**DSC Studies on the Thermotropic Phase Transitions of *N*-Acylglycines.** Heating thermograms of dry NAGs containing even and odd acyl chains are shown in Figure 1A,B, respectively. Each NAG exhibits a major transition that matches well with its melting point. All the NAGs except NMG showed one minor transition before the melting transition, which is most probably due to polymorphism and not because of any impurity since impurities would normally broaden the transition rather than giving rise to separate transitions. The minor transitions disappeared in all cases in the second heating scans and small decreases were noticed in the transition enthalpies. This suggests that during the cooling scans NAGs do not come back to their original structure. Therefore, the first heating scan was considered for further analysis in all cases, and the total area under minor and major transitions was integrated to get the transition enthalpies. Transition temperatures ($T_t$), enthalpies ($\Delta H_t$), and entropies ($\Delta S_t$) of dry NAGs, obtained from the DSC studies, are presented in Table 1.

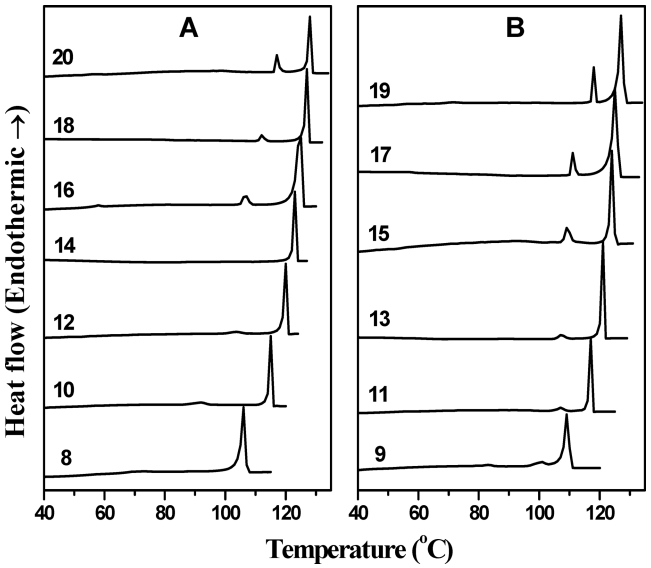


**Figure 1.** DSC heating thermograms of dry NAGs with (A) even and (B) odd number of carbon atoms in the acyl chains. The number of C atoms in the acyl chain is indicated against each thermogram.

Thermograms of hydrated NAGs with even and odd acyl chains are shown in Figure 2A,B, respectively. For each NAG a single sharp peak was seen at ca. 20−40 °C below the phase transition temperature of the dry sample. When the samples were subjected to a second heating scan, small decreases were observed in the transition enthalpies compared with the first scan. Therefore, in all cases, only the first heating scan was considered for further analysis. Values of $T_t$, $\Delta H_t$, and $\Delta S_t$ obtained for hydrated NAGs are also given in Table 1.

**Chain Length Dependence of Thermodynamic Parameters of Dry and Hydrated NAGs.** When the total enthalpy and entropy of the phase transitions (major + minor) of dry NAGs are plotted against the acyl chain length a linear dependence was observed (Figure 3A,B). These data could be fit well to expressions 2 and 3 given below as observed earlier for *N*-acylethanolamines (NAEs) and *N*-acyldopamines with even and odd acyl chain lengths, *O*-acylcholines with even chain lengths, and *N*,*O*-diacylethanolamines (DAEs) with matched as well as mixed acyl chains.[23−26,28,31,32]

$$\Delta H_t = \Delta H_0 + (n - 2)\Delta H_{inc} \quad (2)$$

$$\Delta S_t = \Delta S_0 + (n - 2)\Delta S_{inc} \quad (3)$$

where $n$ is the number of C atoms in the acyl chains and $\Delta H_0$ and $\Delta S_0$ are the end contributions to $\Delta H_t$ and $\Delta S_t$, respectively, arising from the terminal methyl group and the polar region of the NAG molecule. $\Delta H_{inc}$ and $\Delta S_{inc}$ are the average incremental values of $\Delta H_t$ and $\Delta S_t$ contributed by each $CH_2$ group. Linear least-squares analysis of the chain length-dependent values of $\Delta H_t$ and $\Delta S_t$ for homologous series of NAGs yielded the incremental values ($\Delta H_{inc}$ and $\Delta S_{inc}$) and end contributions ($\Delta H_0$ and $\Delta S_0$), which are listed in Table 2. The $\Delta H_{inc}$ and $\Delta S_{inc}$ values observed for the dry NAGs are 0.92 ± 0.03 kcal·mol$^{-1}$ and 2.23 ± 0.08 cal·mol$^{-1}$·K$^{-1}$, respectively.

A linear chain length dependence of the transition enthalpy and transition entropy observed here for the NAGs suggests that structures of the homologous series of NAGs would be quite similar in the solid state. Thus, the molecular packing and intermolecular interactions (e.g., hydrogen bonding) are likely


dx.doi.org/10.1021/cg500481u | Cryst. Growth Des. 2014, 14, 4944−4954

Table 1. Average Values of Transition Temperatures ($T_t$), Transition Enthalpies ($\Delta H_t$), and Transition Entropies ($\Delta S_t$) of NAGs in Dry and Hydrated States[a]

| | dry NAGs | | | hydrated NAGs | | |
|---|---|---|---|---|---|---|
| acyl chain length | $T$ (°C) | $\Delta H_t$ (kcal·mol$^{-1}$) | $\Delta S_t$ (cal·mol$^{-1}$·K$^{-1}$) | $T$ (°C) | $\Delta H_t$ (kcal·mol$^{-1}$) | $\Delta S_t$ (cal·mol$^{-1}$·K$^{-1}$) |
| 8 | 106.4 ± 0.1 | 5.65 ± 0.03 | 14.9 ± 0.1 | 66.15 ± 0.03 | 1.40 ± 0.58 | 4.2 ± 1.7 |
| 9 | 110.1 ± 0.1 | 6.28 ± 0.07 | 16.4 ± 0.1 | 74.07 ± 0.09 | 3.61 ± 0.47 | 10.4 ± 1.4 |
| 10 | 115.6 ± 0.3 | 7.82 ± 0.13 | 20.1 ± 0.3 | 81.47 ± 0.09 | 5.56 ± 0.61 | 15.7 ± 1.7 |
| 11 | 117.3 ± 0.2 | 8.58 ± 0.33 | 21.1 ± 0.8 | 84.86 ± 0.04 | 5.80 ± 0.89 | 16.2 ± 2.5 |
| 12 | 120.4 ± 0.1 | 9.25 ± 0.01 | 23.5 ± 0.1 | 89.21 ± 0.08 | 7.28 ± 0.41 | 20.1 ± 1.1 |
| 13 | 121.6 ± 0.1 | 10.19 ± 0.59 | 25.8 ± 1.5 | 92.31 ± 0.08 | 8.89 ± 0.85 | 24.3 ± 2.3 |
| 14 | 123.8 ± 0.2 | 10.07 ± 0.7 | 25.8 ± 1.8 | 95.19 ± 0.11 | 9.15 ± 0.52 | 24.9 ± 1.4 |
| 15 | 124.6 ± 0.4 | 12.02 ± 0.09 | 30.2 ± 0.2 | 97.71 ± 0.06 | 10.47 ± 0.38 | 28.3 ± 1.0 |
| 16 | 124.9 ± 0.2 | 13.40 ± 0.14 | 32.7 ± 0.4 | 99.83 ± 0.27 | 11.47 ± 0.44 | 30.8 ± 1.2 |
| 17 | 125.7 ± 0.2 | 14.41 ± 0.25 | 36.1 ± 0.6 | 102.16 ± 0.16 | 12.91 ± 0.75 | 34.4 ± 2.0 |
| 18 | 127.3 ± 0.1 | 14.68 ± 0.02 | 36.7 ± 0.1 | 103.90 ± 0.30 | 14.03 ± 0.58 | 37.2 ± 1.5 |
| 19 | 127.6 ± 0.1 | 15.29 ± 0.45 | 38.2 ± 1.1 | 105.73 ± 0.06 | 15.18 ± 1.21 | 40.1 ± 3.2 |
| 20 | 128.8 ± 0.1 | 16.98 ± 0.16 | 42.3 ± 0.4 | 107.67 ± 0.05 | 16.02 ± 1.73 | 42.1 ± 2.5 |

[a]The standard deviations correspond to at least three independent measurements.

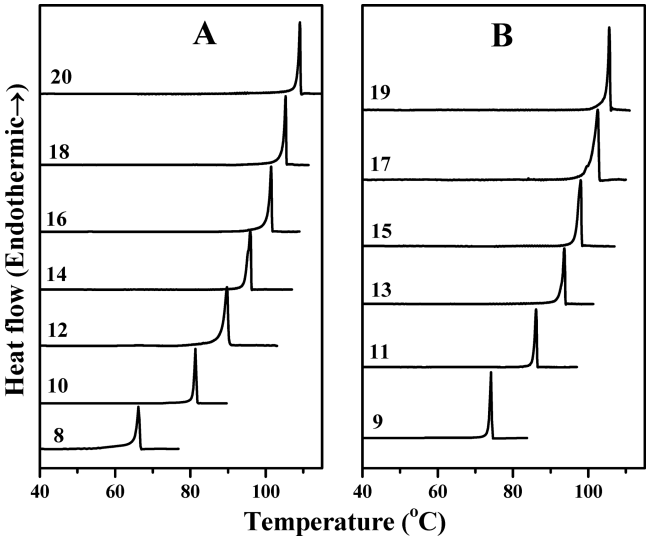


Figure 2. DSC heating thermograms of hydrated NAGs with (A) even and (B) odd number of carbon atoms in the acyl chain. The number of C atoms in the acyl chain is indicated against each thermogram.

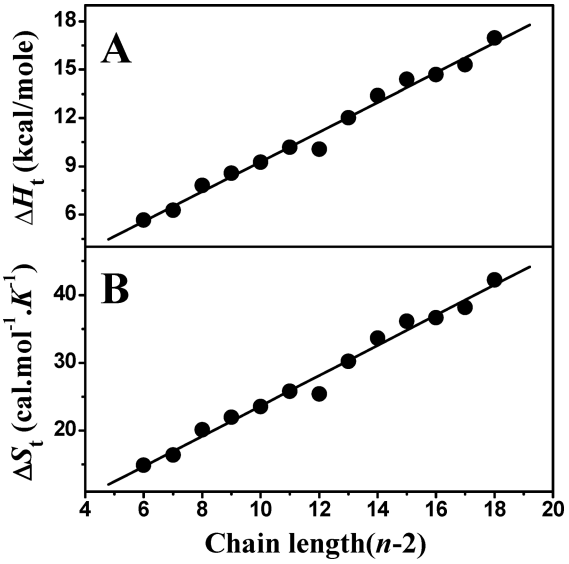


Figure 3. Chain length dependence of (A) transition enthalpies and (B) transition entropies of dry NAGs. Values of $\Delta H_t$ and $\Delta S_t$ were plotted against the number of methylene ($CH_2$) units ($n - 2$) in panels A and B, respectively. Solid lines correspond to linear least-squares fits of the data.

to be very similar in all NAGs in the homologous series. Therefore, determination of the crystal structure of any one NAG should give a reasonably good idea of the molecular packing and intermolecular interactions present in the crystal lattice for the entire homologous series. In the present study, we determined the three-dimensional structure of two different NAGs by single-crystal X-ray diffraction and found that they are isostructural (see below).

Similar to the dry state, upon hydration also NAGs exhibit a linear dependence of transition enthalpy and entropy on their acyl chain length (Figure 4A,B), although the magnitude of these parameters are lower in the hydrated state compared with the dry state. The enthalpy and entropy data of hydrated NAGs also fit well to expressions 2 and 3, as observed earlier for hydrated *N*-acylethanolamines with even and odd acyl chain lengths and *N*-acyldopamines.[24,26,28]

**Thermodynamic Properties and Acyl Chain Tilt.** From Figure 3, it is clear that the enthalpy and entropy corresponding to the chain melting phase transitions of dry NAGs exhibit a linear dependence on the chain length. This is in contrast to the results obtained with a number of long-chain compounds including hydrocarbons, fatty acids, *N*-acylethanolamines, *N*-acyldopamines, and *N*,*O*-diacylethanolamines, all of which exhibit odd−even alternation in the transition enthalpies and entropies.[23−26,32] Such alternation in long chain fatty acids has been explained on the basis of packing of hydrocarbon chains, where differences in the packing of terminal methyl groups between the even and odd acyl chain lengths.[23] Such differences do not arise if the hydrocarbon chains are perpendicular to the methyl group plane. However, if the chains are tilted with respect to the bilayer normal, their packing modes can differ, leading to alternation in the physical properties.[23] Consistent with this, both NAEs and DAEs, which exhibit odd−even alternation, show significant *N*-acyl chain tilt (~34−37° with respect to the bilayer normal).[25,32−35] On the other hand, the acyl chains in NAGs are nearly perpendicular to the bilayer plane with very small tilt angles of 0.03° and 0.84°


dx.doi.org/10.1021/cg500481u | Cryst. Growth Des. 2014, 14, 4944−4954

Table 2. Incremental Values ($\Delta H_{inc}$, $\Delta S_{inc}$) of Chain Length Dependence and End Contributions ($\Delta H_0$, $\Delta S_0$) to Phase Transition Enthalpy and Entropy of NAGs[a]

| | $\Delta H_{inc}$ (kcal·mol$^{-1}$) | $\Delta H_0$ (kcal·mol$^{-1}$) | $\Delta S_{inc}$ (cal·mol$^{-1}$·K$^{-1}$) | $\Delta S_0$ (cal·mol$^{-1}$·K$^{-1}$) |
|---|---|---|---|---|
| dry NAGs | 0.92 ± 0.03 | 0.42 ± 0.41 | 2.23 ± 0.08 | 1.29 ± 1.05 |
| hydrated NAGs | 1.15 ± 0.03 | −4.34 ± 0.35 | 2.95 ± 0.08 | −10.06 ± 1.05 |

[a]Average values of transition enthalpy and transition entropy given in Table 1 have been used for the linear fitting of the data. Errors are fitting errors obtained from the linear least squares analysis.

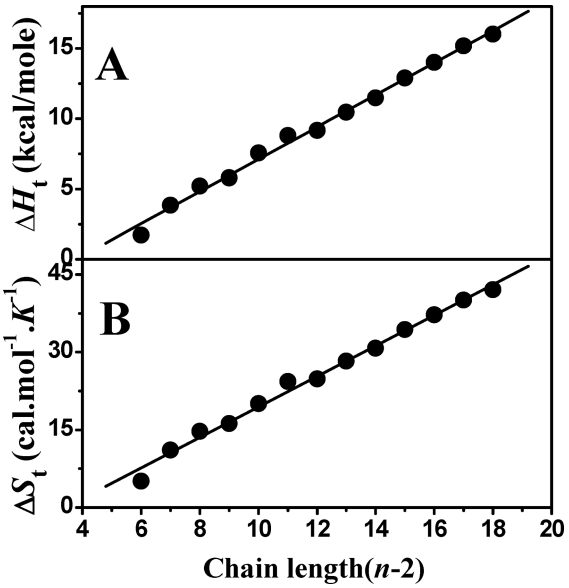


Figure 4. Chain length dependence of (A) transition enthalpies and (B) transition entropies of hydrated NAGs. Values of $\Delta H_t$ and $\Delta S_t$ were plotted against the number of methylene ($CH_2$) units ($n - 2$) in panels A and B, respectively. Solid lines correspond to linear least-squares fits.

for NMG and NPG, respectively (see below). These observations are consistent with the observed linear dependence of transition enthalpies and entropies of the homologous series of dry NAGs.

**Incremental Values of Transition Enthalpy and Entropy.** Linear least-squares analysis of transition enthalpies and transition entropies of NAGs in the dry and hydrated states yielded incremental values ($\Delta H_{inc}$ and $\Delta S_{inc}$) and end contribution ($\Delta H_0$ and $\Delta S_0$). It is observed that the value of $\Delta H_{inc}$ of dry NAGs is slightly lower than the $\Delta H_{inc}$ corresponding to the hydrated state. But, in case of NAEs it was found that $\Delta H_{inc}$ of dry state is higher than that of the hydrated state. The end contribution of entropy, $\Delta S_0$, is also more negative for hydrated samples compared with the dry samples.[24,28,36] The higher $\Delta H_{inc}$ of hydrated NAGs compared with the dry samples and larger negative $\Delta S_0$ of higher NAGs are indicative of the hydrophobic effect playing a role in the packing of NAGs, which could arise due to the ordering of water molecules around the carboxylic acid moiety of the headgroup.[37] Therefore, it appears that the hydrophobic effect in hydrated form brings the NAG molecules closer, resulting in a tight packing of the acyl chains.

The acyl chain tilt with respect to the bilayer normal in NAGs is in the neighborhood of zero, whereas in NAEs it is around 35−37°,[36] which is in agreement with the higher $\Delta H_{inc}$ for NAGs, in the dry and hydrated states. This suggests that the acyl chains are packed more closely in NAGs than in NAEs.

**Chain Length Dependence of Phase Transition Temperatures of NAGs.** The transition temperatures of dry as well as hydrated NAGs increase with increasing chain length as shown in Figure 5, but the magnitude of the change

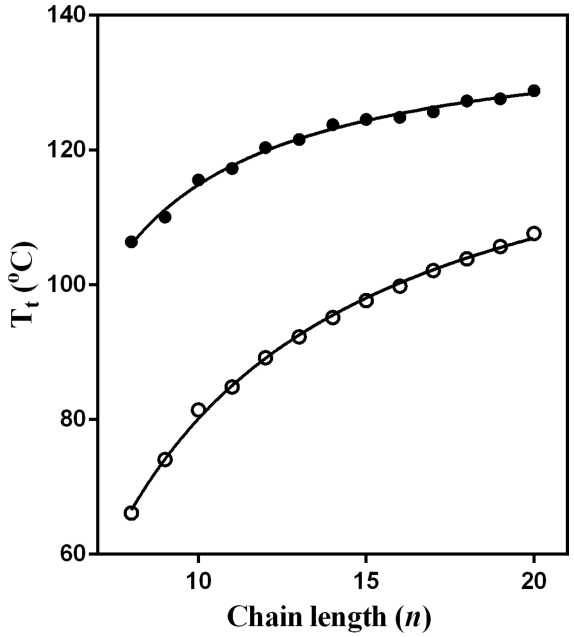


Figure 5. Chain length dependence of chain-melting phase transition temperatures of NAGs in the dry (●) and hydrated (○) states. Solid lines correspond to nonlinear least-squares fit of the transition temperatures to eq 7.

decreases with increase in the chain length. When the acyl chain length is increased, the total contribution from the polymethylene portion toward the total enthalpy and entropy of the phase transition also increases, whereas the end contributions remain constant. Therefore, at infinite acyl chain length, the end contributions become insignificant compared with the contribution from the polymethylene portion. Consequently, the end contributions can be neglected, which reduces eqs 2 and 3 to[23]

$$\Delta H_t = (n - 2)\Delta H_{inc} \quad (4)$$

$$\Delta S_t = (n - 2)\Delta S_{inc} \quad (5)$$

Then the transition temperature for infinite chain length, $T_t^{\infty}$, will be given by

$$T_t^{\infty} = \Delta H_{inc}/\Delta S_{inc} \quad (6)$$

From the data presented in Table 2 and using eq 6, the $T_t^{\infty}$ values for NAGs in the dry and hydrated state have been estimated as 412.6 and 389.8 K, respectively.

For a number of single-chain as well as two-chain lipids, which exhibit linear dependence of $\Delta H_t$ and $\Delta S_t$ on chain


dx.doi.org/10.1021/cg500481u | Cryst. Growth Des. 2014, 14, 4944−4954

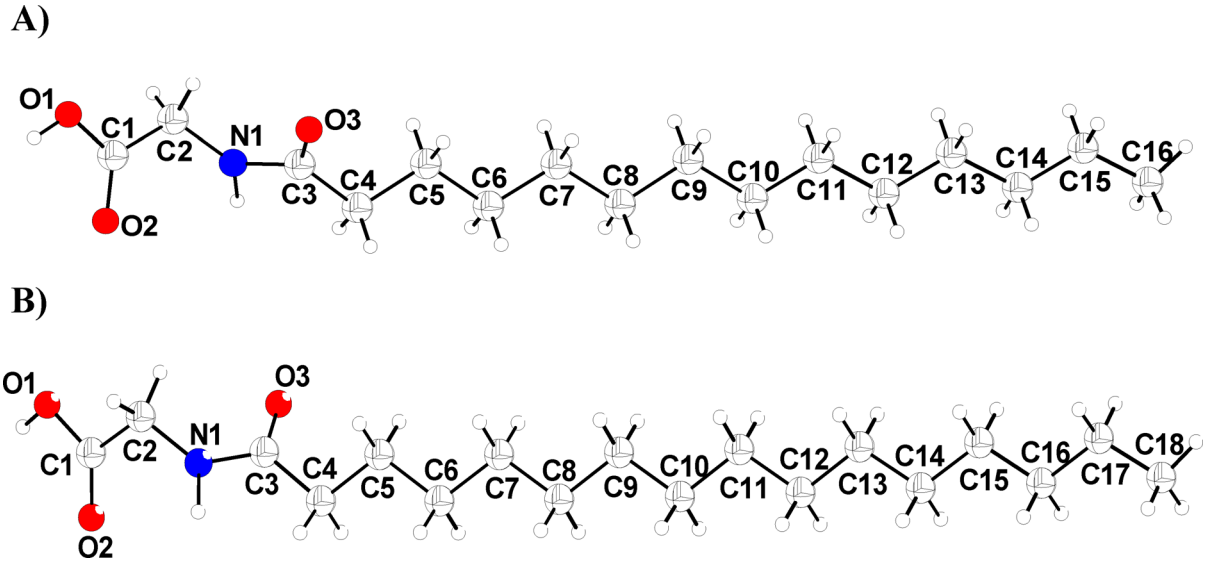


**Figure 6.** ORTEPs showing the molecular structures of (A) *N*-myristoylglycine and (B) *N*-palmitoylglycine.

length, it has been shown that the transition temperature data can be fit to the following equation:[38]

$$T_t = \Delta H_t/\Delta S_t = T_t^{\infty}[1 - (n_0 - n_0')/(n - n_0')] \quad (7)$$

where $n_0$ (= $-\Delta H_0/\Delta H_{inc}$) and $n_0'$ (= $-\Delta S_0/\Delta S_{inc}$) are the values of $n$ at which the transition enthalpy and transition entropy extrapolate to zero. Figure 5 shows that the $T_t$ values of NAGs investigated here fit very well with eq 7, in the dry and hydrated states. The fitting parameters also yielded the $T_t^{\infty}$ values for NAGs in the dry and hydrated states as 411.4 ± 1.4 K and 406.6 ± 2.1 K, respectively. These values are in good agreement with the $T_t^{\infty}$ values estimated using eq 6.

**Crystal Structures of NMG and NPG.** ORTEPs of *N*-myristoylglycine and *N*-palmitoylglycine are shown in Figure 6A,B, respectively, along with the atom numbering for all non-hydrogen atoms. The crystal parameters of NMG are given in Table 3, and the atomic coordinates and equivalent isotropic displacement parameters for all non-hydrogen atoms are given in Table S4, Supporting Information. The bond distances and bond angles involving all non-hydrogen atoms are given in Table S5, Supporting Information, and selected torsion angles are given in Table S6, Supporting Information. Corresponding data for NPG are given in Tables S7−S9, Supporting Information. The ORTEPs in Figure 6 indicate that both NMG and NPG adopt an essentially linear geometry. This is consistent with the torsion angles observed in the hydrophobic region (Tables S6 and S9, Supporting Information), which are very close to 180°, clearly indicating that the nonpolar portion (C3−C18) of the acyl chain is in all-*trans* conformation in both these compounds. In addition, the carbonyl oxygen and amide N−H are also in *trans* geometry in both compounds.

**Table 3. Crystallographic Data for *N*-Myristoylglycine and *N*-Palmitoylglycine at 298 K**

| crystal parameters | NMG | NPG |
|---|---|---|
| formula | $C_{16}H_{31}NO_3$ | $C_{18}H_{35}NO_3$ |
| formula wt | 285.42 | 313.47 |
| cryst syst | monoclinic | monoclinic |
| space group | *C*2/*c* | *P*21/*c* |
| *a* (Å) | 92.388(16) | 51.343(9) |
| *b* (Å) | 4.86(8) | 4.8679(8) |
| *c* (Å) | 7.6485(13) | 7.6195(13) |
| *α* (deg) | 90.00 | 90.00 |
| *β* (deg) | 91.702(4) | 92.830(3) |
| *γ* (deg) | 90.00 | 90.00 |
| *Z* | 8 | 4 |
| *V* (Å$^3$) | 3432.7(10) | 1902.0(6) |
| $D_{calc}$ (g cm$^{-3}$) | 1.105 | 1.095 |
| $R_1$ | 8.05 | 8.74 |
| $wR_2$ | 20.72 | 24.4 |
| GOF | 1.115 | 1.167 |
| data completeness | 99.0% | 96.1% |

**Molecular Packing, Hydrogen Bonding, and Intermolecular Interactions.** A packing diagram of NPG viewed down the *c*-axis is shown in Figure 7A and close-up views of the hydrogen bonding interactions as seen down the *c*-axis and *b*-axis are shown in Figure 7B,C, respectively. From this figure, it can be seen that NPG molecules are packed in a head-to-head (and tail-to-tail) fashion in stacked bilayers. The carboxylic acid groups from opposite leaflets associate via O−H···O hydrogen bonds, leading to the formation of eight-membered cyclic structures connecting two leaflets from adjacent bilayers. Additionally, the amide groups of adjacent molecules in the same leaflet are also involved in hydrogen bonding. The methyl ends of stacked bilayers are in van der Waals' contacts, and the methyl ends from opposite leaflets face each other with the closest methyl−methyl distance between opposite layers being 4.008 Å and that within the same leaflet being 4.868 Å. The bilayer thickness (i.e., O1−O1 distance) in the NPG crystal lattice is 49.954 Å, whereas the monolayer (single leaflet) thickness (O1−C18 distance) is 23.387 Å. The repeat distance (*d*-spacing) is 51.28 Å. The all-*trans* acyl chains are tilted by 0.84° with respect to the bilayer normal.

Packing diagrams of NMG viewed down the *c*-axis and *b*-axis are shown in Figure S4A,B, Supporting Information, respectively. Similar to NPG, NMG molecules are also packed in a head-to-head fashion, akin to that found in phospholipid bilayers. The molecular packing and intermolecular interactions are essentially similar to those found in the crystal structure of NPG, described above. Only minor differences are seen as indicated below. The closest methyl−methyl distances between


dx.doi.org/10.1021/cg500481u | *Cryst. Growth Des.* 2014, 14, 4944−4954

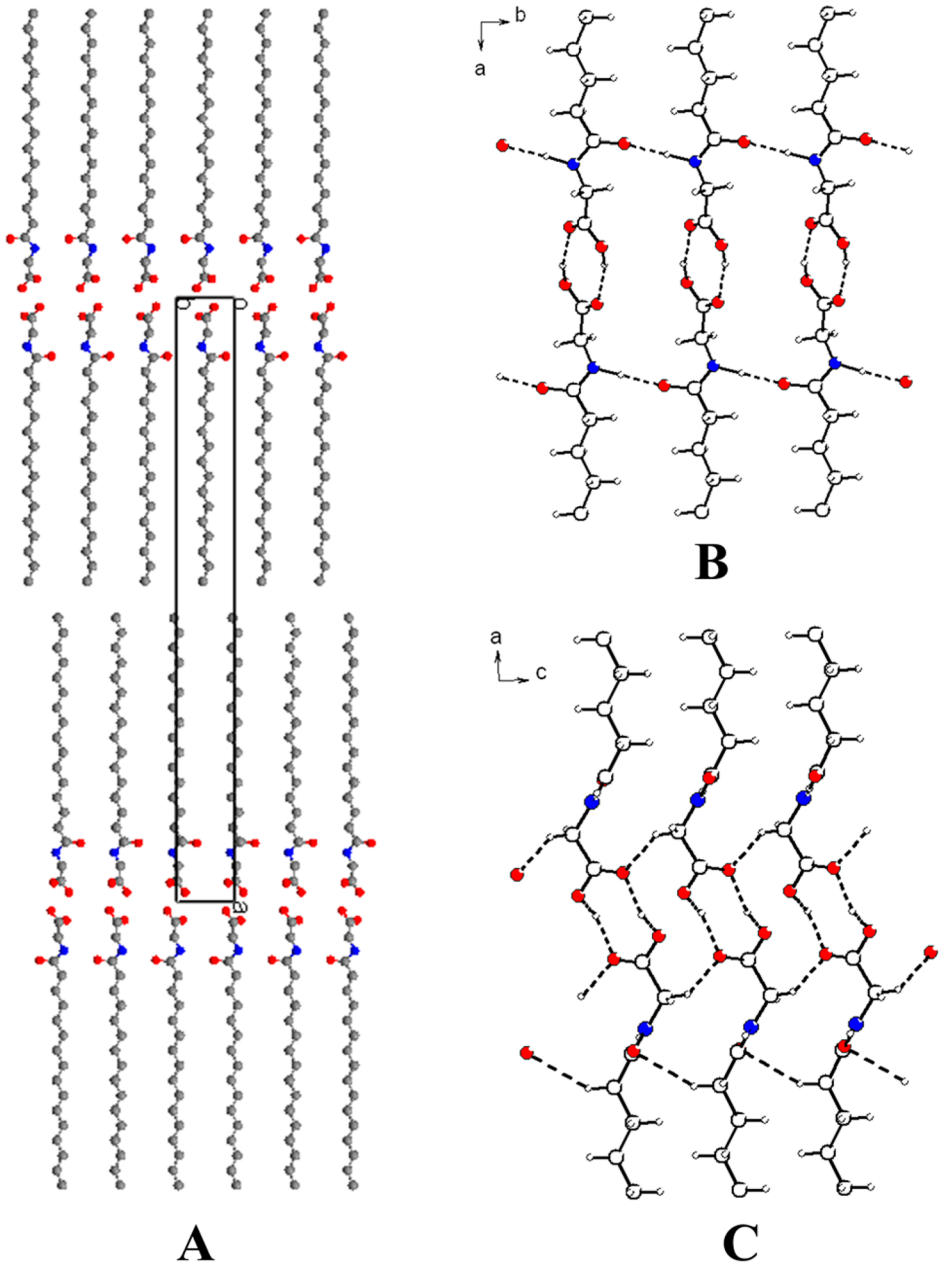


**Figure 7.** Packing diagrams of *N*-palmitoylglycine indicating the bilayer arrangement and hydrogen bonding networks. (A) A view of the bilayer arrangement in NPG. (B) A view down the *c*-axis depicting the O−H···O and N−H···O type hydrogen bonds. (C) A view down the *b*-axis, depicting the O−H···O and C−H···O type hydrogen bonds. Atom code: carbon, large open circle; nitrogen, blue circle; oxygen, red circle; hydrogen, small open circle.

opposite layers and within the same leaflet in NMG are 3.73 and 4.86 Å, respectively. The bilayer thickness (O1−O1 distance) and monolayer thickness (O1−C16 distance) are 44.61 and 20.86 Å, respectively. The repeat distance (*d*-spacing) is 46.17 Å. The all-*trans* acyl chains are tilted with respect to bilayer normal by 0.03°, which is very close to that observed in the crystal structure of NPG. The acyl chain tilt observed in the NAGs is negligible compared with that observed in *N*-acylethanolamines (ca. 35−37°).[33−35] These observations are consistent with a lack of odd−even alternation in the thermodynamic parameters determined from DSC studies, discussed above.

An examination of Figure 7B shows that the O−H···O hydrogen bonds form a cyclic structure, with each carboxylic acid group being involved in two hydrogen bonds with an NPG molecule from the opposite leaflet. Here, each carboxylic acid group acts both as a proton donor and as a proton acceptor with the carboxylic acid group of another molecule in the opposite layer. The H···O distance in the O−H···O hydrogen bonds is 1.742 Å, whereas the distance between the donor and acceptor oxygen atoms is 2.686 Å, and the bond angle subtended at the hydrogen atom is 156.34°. Besides the hydrogen bonds between the carboxyl groups, strong hydrogen bonds are also formed between the amide N−H and carbonyl oxygen of adjacent NPG molecules (Figure 7B). While the N−H group of each NPG molecule forms a hydrogen bond with another NPG molecule in the adjacent unit cell on one side, the carbonyl oxygen of the same molecule forms a hydrogen bond


dx.doi.org/10.1021/cg500481u | *Cryst. Growth Des.* 2014, 14, 4944−4954

with the amide N−H of another NPG molecule in the adjacent unit cell on the other side. All these hydrogen bonds are also identical, with a N−O distance of 2.974 Å, a H···O distance of 1.808 Å, and a N−H···O angle of 177.99°. Similar N−H···O hydrogen bonds have been observed in the crystal structures of a number of amphiphiles including *N*-acylethanolamines, *N,O*-diacylethanolamines, and *N*-acyldopamines and in *N,N,N″*-tris(*n*-octyl)benzene-1,3,5-tricarboxamide, a C3-symmetric triamide with three alkyl chains.[25,26,32−35,39]

The hydrogen bonding pattern in the crystal lattice of NMG viewed down the *c*-axis and *b*-axis are shown in Figure S5A,B, Supporting Information, respectively. From this figure, it can be clearly seen that the hydrogen bonding patterns in the NMG crystal lattice are very similar to those observed in the crystal lattice of NPG. All of the O−H···O hydrogen bonds in NMG are identical, with an O−O distance of 2.684 Å, an O···H distance of 1.721 Å, and a hydrogen bond angle of 168.34°. Similar to that observed in the crystal structure of NPG, all of the N−H···O hydrogen bonds in NMG are also identical, with an O···H bond length of 2.091 Å, a N−O distances of 2.963 Å, and a hydrogen bond angle of 164.77°. In both cases, donut shaped structures are formed by the hydrogen bonded carboxylic acid dimers. This is shown for NPG in Figure S6, Supporting Information.

In addition to the O−H···O and N−H···O hydrogen bonds, weak C−H···O hydrogen bonds have been observed in the crystal structures of NMG and NPG. Hydrogen bonds with interaction energies up to −5 kcal·mol$^{-1}$ are generally considered weak hydrogen bonds, and many examples of this type have been described earlier.[40−43] Figure 7C gives a view of four sets of C−H···O type hydrogen bonds observed in the crystal lattice of NPG. The C−H···O hydrogen bonds between C2−H and O2 are of two types. These bonds are formed between O2 (oxygen atom of carboxylic carbonyl group) of one molecule with two different H atoms (H2A and H2B) on C2 (carbon atom $\alpha$ to the carboxylic carbonyl) of the adjacent molecule in the same layer. All the C2(H2A)···O2 bonds are identical, with a C2(H2A)−O2 distance of 3.743(3) Å, an H2A···O2 distance of 3.074 Å, and a C2−H2A···O2 angle of 129.8°. Similarly, all the C2(H2B)···O2 bonds are also identical, with a C2(H2B)−O2 distance of 3.248 Å, an H2B···O2 distance of 2.406 Å, and C2−H2B···O2 angle of 144.8°. These C2(H2B)···O2 hydrogen bonds are considerably stronger than the C2(H2A)···O2 hydrogen bonds. Stabilization of lipid membrane structure by C−H···O hydrogen bonds has been reported earlier for the paraffinic ylide trimethylammonio *n*-hexadecylsulfonamidate.[44]

Other C−H···O hydrogen bonds between C4−H and O3 are of two types. These bonds are formed between O3 (oxygen atom of amide carbonyl group) of one molecule with H atoms on C4 (carbon atom $\alpha$ to the amide carbonyl) of the adjacent molecule in the same layer (Figure 7C). All the C4(H4A)···O3 bonds are identical, with a C4(H4A)−O3 distance of 3.487 Å (3), an H4A···O3 distance of 2.62 Å, and a C4−H4A···O3 angle of 149°. Similarly, all the C4(H4B)···O3 bonds are also identical, with a C4(H4B)−O3 distance of 5.228 Å, an H4B···O3 distance of 4.59 Å, and a C4−H4B···O3 angle of 126.6°. Very similar C−H···O hydrogen bonds were observed in the crystal lattice of NMG (see Figure S5B and associated description in the Supporting Information).

**Molecular Area.** The area per molecule in the bilayer plane in the crystal lattice of NMG and NPG is 18.59 and 18.55 Å$^2$, respectively. These values are less than those found for NAEs whose three-dimensional structures have been determined earlier, namely, *N*-myristoylethanolamine (21.95 Å$^2$), *N*-palmitoylethanolamine (polymorphs $\alpha$ and $\beta$, 21.99 Å$^2$ and 22.03 Å$^2$, respectively), and *N*-stearoylethanolamine (21.99 Å$^2$), as well as some other single-chain lipids such as 3(11-bromoundecanoyl)-D-glycerol, 3-lauroyl-D-glycerol, and 3-stearoyl-D-glycerol, whose molecular areas are in the range of 21.5−22.7 Å$^2$.[33−35,45−48] The smaller molecular area of NAGs is due to their small headgroup size and negligible acyl chain tilt with respect to the bilayer normal. Other single chain lipids such as lysophosphatidic acid and lysophosphatidylethanolamine have somewhat larger areas (33.6 and 34.8 Å$^2$, respectively). Such large molecular areas observed in these two molecules are in part due to the very high tilt in the acyl chains with respect to bilayer normal and large hydrophilic head groups.[49,50]

**Powder X-ray Diffraction Studies.** Additional insights into the molecular packing of NAGs with different acyl chains were obtained from powder X-ray diffraction studies. PXRD profiles of NAGs with different acyl chain lengths investigated here are shown in Figure 8A,B. All the NAGs gave sharp

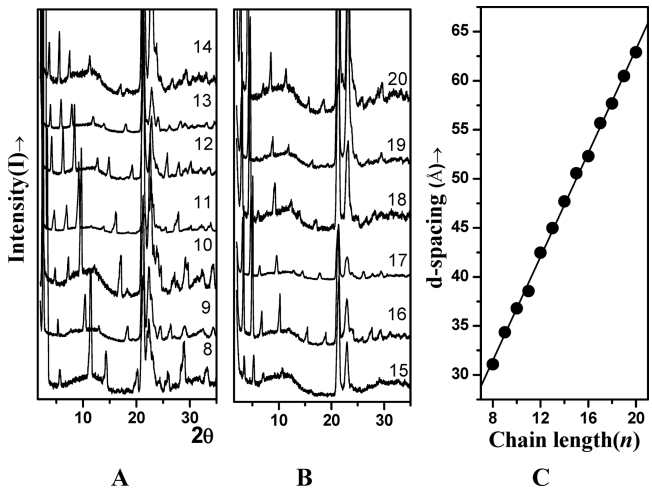


**Figure 8.** Powder X-ray diffraction patterns of *N*-acylglycines with different saturated acyl chains (A, B) and dependence of *d*-spacings on the acyl chain length (C). The number of carbon atoms in the saturated unbranched acyl chains is indicated against each PXRD profile. The solid line in panel C is a linear least-squares fit of the data. The slope of this line yielded increase in the *d*-spacing per each additional $CH_2$ unit as 1.323 Å.

diffraction peaks that were consistent with lamellar packing of the acyl chains. From the position of the peaks, the *d*-spacings were calculated, and in each case 4−6 peaks were used for estimating the *d*-spacing. The values obtained are presented in Table S10, Supporting Information. The *d*-spacings obtained for NMG and NPG from the PXRD data (47.69 and 52.31 Å, respectively) are in good agreement with the values obtained from the single crystal X-ray diffraction (46.17 and 51.28 Å, respectively).

A plot depicting the chain length dependence of the *d*-spacing (Figure 8C) is linear with a slope of 2.645 Å, which corresponds to an increment of 1.323 Å per additional $CH_2$ moiety in each chain. This is consistent with the observation of untilted bilayer packing observed in the crystal structures of NMG and NPG. The linear dependence of the *d*-spacings on the acyl chain length suggests that all the NAGs pack in a


dx.doi.org/10.1021/cg500481u | *Cryst. Growth Des.* 2014, 14, 4944−4954

similar manner in the solid state. That is, in the solid state all the NAGs would adopt a bilayer structure with chains packed in an essentially untilted fashion (with respect to the bilayer normal).

**Polymorphism in *N*-Acylglycines in the Solid State.** As indicated in the section DSC Studies on the Thermotropic Phase Transitions of N-Acylglycines, DSC studies show that all the NAGs (except NMG) studied here show a minor endothermic phase transition in addition to the major transition, which corresponds to the capillary melting point of the compound. This additional transition is most likely due to conversion of one solid form to another and suggests the presence of structural polymorphism in NAGs. In order to investigate this in greater detail, we carried out variable temperature powder X-ray diffraction (VT-PXRD) and FTIR studies. PXRD patterns of NPG recorded at different temperatures are shown in Figure 9A. It may be noted that the DSC thermogram of NPG shows a minor transition at 107 °C and a melting transition at 124.95 °C (see Figure 1 and Table 1). The PXRD patterns recorded at 27 and 105 °C are essentially identical indicating that no changes occur in the solid state structure of this compound below 105 °C. However, upon heating to 110 °C, additional peaks are seen in the PXRD data, suggesting that significant changes occur in the solid state structure of NPG during the minor transition. No additional changes are seen upon further heating to 120 °C, whereas all the peaks in the PXRD pattern disappear when the sample was further heated to 125 °C, consistent with the liquid state of the sample above the phase transition. We refer to the phase present below 107 °C as form-I and that seen above 107 °C as form-II. A comparison of the simulated PXRD pattern derived from the structure of NPG determined by single-crystal X-ray diffraction with the PXRD patterns obtained at 27 and 115 °C (Figure 9B) shows a good correlation between the simulated PXRD pattern and that of form-II. This shows that the single crystal of NPG used in the X-ray diffraction study corresponds to form-II. Since single crystals of form-I could not be obtained for any of the NAGs, we carried out FT-IR spectroscopic studies in order to obtain additional insights into their solid-state polymorphism, with NPG as a representative example. FTIR spectra of NPG recorded at different temperatures are shown in Figure S7, Supporting Information The spectrum recorded at room temperature (ca. 25 °C), shows two IR bands around ~1705 and ~1740 $cm^{-1}$ for the carboxylic acid moiety, whereas the spectrum recorded after the sample was heated to 115 °C and cooled to room temperature (which is above the minor solid-to-solid phase transition; see Figure 1) shows only one band in the carbonyl stretching region at ~1705 $cm^{-1}$, which is consistent with a change in the crystal form. A similar spectrum was obtained after heating the sample to 135 °C followed by cooling to room temperature, suggesting that only form-II is obtained when the molten NPG undergoes liquid–solid phase transition. This observation is in good agreement with DSC and VT-PXRD studies.

The DSC thermogram of *N*-pentadecanoylglycine (NPDG) shows a minor transition at 109.5 °C, in addition to the melting transition at 124.6 °C. The minor transition therefore corresponds to a solid–solid phase transition and clearly indicates that NPDG also exhibits polymorphism. This interpretation is further supported by VT-PXRD, which showed additional diffraction peaks at 120 °C (Figure S8, Supporting Information). In contrast to other even acyl chain length NAGs, NMG gives only one phase transition, which

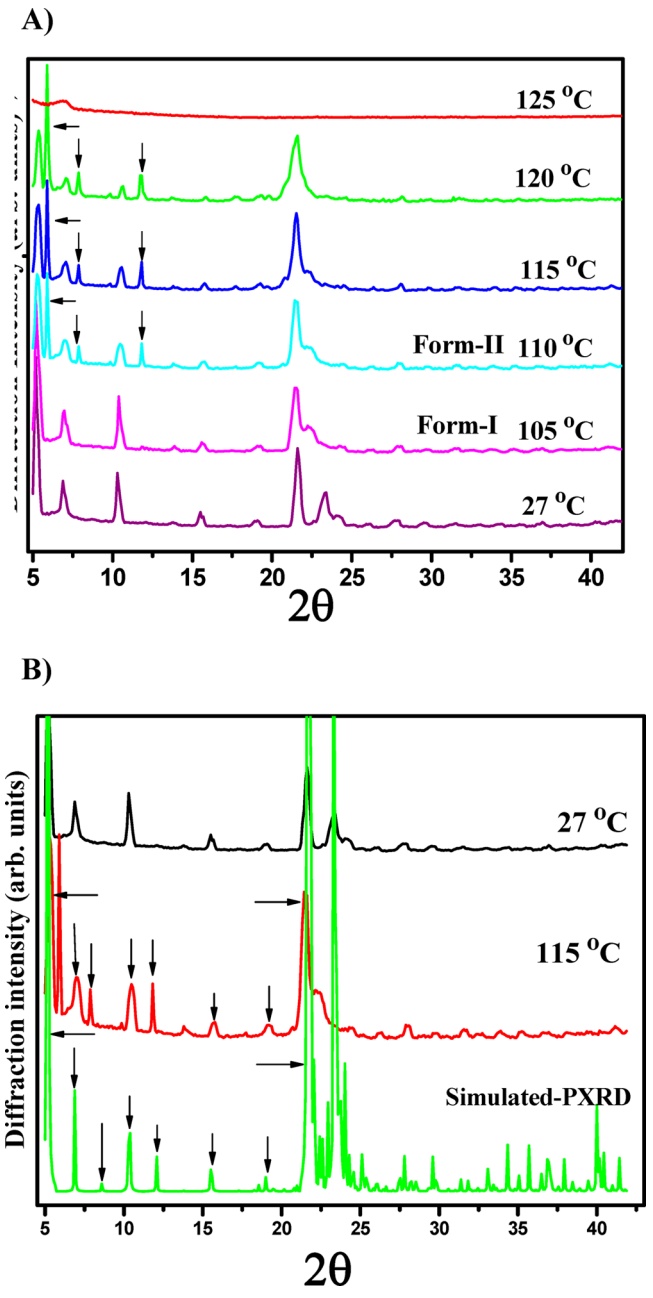


**Figure 9.** (A) Variable temperature powder X-ray diffraction patterns (VT-PXRD) of dry *N*-palmitoylglycine. The temperature at which each scan was recorded is indicated in the figure. (B) Comparison of simulated PXRD pattern of NPG obtained from single-crystal XRD with experimental VT-PXRD pattern of NPG.

corresponds to the melting transition (Figure 1). The VT-PXRD pattern of NMG does not show any detectable changes when heated from room temperature to the phase transition temperature (data not shown). In addition to these, the FTIR spectrum of NMG gave only one carbonyl band at ~1700 $cm^{-1}$ corresponding to the carboxylic acid moiety (Figure S9, Supporting Information). These observations suggest that polymorphism could not be detected in the solid state of NMG.

**Biological Implications and Future Directions.** Results obtained in the present studies show that NAGs exhibit significantly higher phase transition temperatures compared with diacylphospholipids such as phosphatidylcholines and phosphatidylethanolamines of similar acyl chain lengths and


dx.doi.org/10.1021/cg500481u | *Cryst. Growth Des.* 2014, 14, 4944–4954

that they pack in a bilayer format. This suggests that NAGs would most likely stabilize the membrane structure when incorporated into phospholipid bilayers. The crystal structures of NMG and NPG show that the acyl chains in these molecules are oriented essentially perpendicular to the bilayer plane, which would be the least disturbing way to accommodate them into the host matrix. The hydrogen bonding capability of the amide moiety at the hydrophobic−hydrophilic interface of the NAG molecule could provide potential interaction with other membrane consituents such as phospholipids, glycolipids, cholesterol, and integral proteins. The carboxyl group of the glycine moiety can potentially exhibit electrostatic interactions with peripheral proteins. Such interactions could be relevant to the biological roles of NAGs, for example, antinociceptive activity.

## SUMMARY AND CONCLUSIONS

In the present study, we have synthesized a homologous series of *N*-acylglycines, which are naturally occurring amphiphiles present in the neural tissues of mammals, and characterized their thermotropic phase behavior and structure by differential scanning calorimetry and X-ray diffraction. Most NAGs showed a minor transition before the chain-melting transition, indicating the possibility of polymorphism. Analysis of the DSC results indicated that the thermodynamic parameters, $\Delta H_t$ and $\Delta S_t$, exhibit a linear dependence on the chain length both in the dry state and upon hydration, lacking the characteristic odd−even alternation observed with a number of other single-chain amphiphiles, which could be explained on the basis of the crystal structures of *N*-myristoylglycine and *N*-palmitoylglycine, wherein the NAGs adopt an extended geometry, with the molecules packed in a bilayer fashion in the crystal lattice with the acyl chains oriented essentially perpendicular to the bilayer plane. Powder X-ray diffraction data suggest that in the solid state all the NAGs in the homologous series investigated ($n$ = 8−20) adopt a very similar packing arrangement. These studies provide a thermodynamic and structural basis for understanding the functional roles of *N*-acylglycines in the parent tissues where they occur. Especially, the present results will be relevant to understand their interaction with other constituents of biomembranes such as integral membrane proteins, as well as major membrane lipids, such as phospholipids and cholesterol. Future studies from our laboratory will focus on these aspects.

## ASSOCIATED CONTENT

### Supporting Information

Assignment of IR resonances, $^1$H and $^{13}$C NMR data, and *d*-spacings for NAGs, atomic coordinate and isotropic displacement parameters, selected bond distances and angles, and torsion angles for NMG and NPG, representative IR, NMR, PXRD, and hydrogen bonding data for select NAGs, and crystallographic information in CIF format. This material is available free of charge via Internet at http://pubs.acs.org.

## AUTHOR INFORMATION

### Corresponding Author

*Prof. Musti J. Swamy. Tel: +91-40-2313-4807. Fax: +91-40-2301-2460. E-mail: mjssc@uohyd.ernet.in; mjswamy1@gmail.com.

### Notes

The authors declare no competing financial interest.

## ACKNOWLEDGMENTS

This work was supported by a research grant from the Department of Science and Technology (India) to M.J.S. S.T.R. is a Senior Research Fellow of the Council of Scientific and Industrial Research (India). K.P.K. was supported by a D. S. Kothari postdoctoral fellowship from the University Grants Commission (India). Use of the National Single Crystal Diffractometer Facility at the School of Chemistry, University of Hyderabad, funded by the DST (India), is gratefully acknowledged. The UGC (India) is acknowledged for their support through the UPE and CAS programs to the University of Hyderabad and School of Chemistry, respectively.

## REFERENCES

(1) Cartwright, N. J. *Biochem. J.* **1955**, *60*, 238−242.
(2) Schmid, H. H. O.; Schmid, P. C.; Natarajan, V. *Prog. Lipid Res.* **1990**, *29*, 1−43.
(3) Huang, S. M.; Bisogno, T.; Trevisani, M.; Al-Hayani, A.; de Petrocellis, L.; Fezza, F.; et al. *Proc. Natl. Acad. Sci. U.S.A.* **2002**, *99*, 8400−8405.
(4) Cravatt, B. F.; Prospero-Garcia, O.; Siuzdak, G.; Gilula, N. B.; Henriksen, S. J.; Boger, D. L.; Lerner, R. A. *Science* **1995**, *268*, 1506−1509.
(5) Connor, M.; Vaughn, C. W.; Vandenberg, R. J. *Br. J. Pharmacol.* **2010**, *160*, 1857−1871.
(6) Devane, W. A.; Hanus, L.; Breuer, A.; Pertwee, R. G.; Stevenson, L. A.; Griffin, G.; Gibson, D.; Mandelbaum, A.; Etinger, A.; Mechoulam, R. *Science* **1992**, *258*, 1946−1949.
(7) Scheul, H.; Goldstein, E.; Mechoulam, R.; Zimmerman, A. M.; Zimmerman, S. *Proc. Natl. Acad. Sci. U.S.A.* **1994**, *91*, 7678−7682.
(8) Venance, L.; Piomelli, D.; Glowinski, J.; Giaume, C. *Nature* **1995**, *376*, 590−594.
(9) Sheskin, T.; Hanus, L.; Slager, J.; Vogel, Z.; Mechoulam, R. *J. Med. Chem.* **1997**, *40*, 659−667.
(10) Huang, S. M.; Bisogno, T.; Petros, T. J.; Chang, S. Y.; Zavitsanos, P. A.; Zipkin, R. E.; Sivakumar, R.; Coop, A.; Maeda, D. Y.; Petrocellis, L. D.; et al. *J. Biol. Chem.* **2001**, *276*, 42639−42644.
(11) Bradshaw, H. B.; Walker, J. M. *Br. J. Pharmacol.* **2005**, *144*, 459−465.
(12) Hohmann, A. G.; Suplita, R. L.; Bolton, N. M.; Neely, M. H.; Fegley, D.; Mangieri, R.; Krey, J. F.; Walker, J. M.; Holmes, P. V.; Crystal, J. D.; et al. *Nature* **2005**, *435*, 1108−1112.
(13) Succar, R.; Mitchell, V. A.; Vaughan, C. W. *Mol. Pain* **2007**, *3*, 24.
(14) Vuong, L. A.; Mitchell, V. A.; Vaughan, C. W. *Neuropharmacology* **2008**, *54*, 189−193.
(15) Kohno, M.; Hasegawa, H.; Inoue, A.; Muraoka, M.; Miyazaki, T.; Oka, K.; Yasukawa, M. *Biochem. Biophys. Res. Commun.* **2006**, *347*, 827−832.
(16) Burstein, S. H.; Huang, S. M.; Petros, T. J.; Rossetti, R. G.; Walker, J. M.; Zurier, R. B. *Biochem. Pharmacol.* **2002**, *64*, 1147−1150.
(17) Wiles, A. L.; Pearlman, R.-J.; Mari Rosvall, M.; Aubrey, K. R.; Vandenberg, R. J. *J. Neurochem.* **2006**, *99*, 781−786.
(18) Bradshaw, H. B.; Rimmerman, N.; Hu, S. S.-J.; Benton, V. M.; Stuart, J. M.; Masuda, K.; Cravatt, B. F.; O'Dell, D. K.; Walker, J. M. *BMC Biochem.* **2009**, *10*, 14.
(19) Rimmerman, N.; Bradshaw, H. B.; Hughes, H. V.; Chen, J. S.-C.; Hu, S. S. −J; McHugh, D.; Vefring, E.; Jahnsen, J. A.; Thompson, E. L.; Masuda, K.; et al. *Mol. Pharmacol.* **2008**, *74*, 213−224.
(20) Bradshaw, H. B.; Rimmerman, N.; Hu, S. S.-J.; Burstein, S.; Walker, J. M. *Vitam. Horm.* **2009**, *81*, 191−205.
(21) Tan, B.; Yu, Y. W.; Monn, M. F.; Hughes, H. V.; O'Dell, D. K.; Walker, J. M. *J. Chromatogr. B* **2009**, *877*, 2890−2894.
(22) Tan, B.; O'Dell, D. K.; Yu, Y. W.; Monn, M. F.; Hughes, H. V.; Burstein, S.; Walker, J. M. *J. Lipid Res.* **2010**, *51*, 112−119.
(23) Larsson, K. In *Physical Properties−Structural and Physical Characteristics. The Lipid Handbook*; Gunstone, F. D., Harwood, J.

L., Padley, F. B., Eds.; Chapman and Hall: London, 1986; pp 321−384.
(24) Ramakrishnan, M.; Swamy, M. J. *Chem. Phys. Lipids* **1998**, *94*, 43−51.
(25) Kamlekar, R. K.; Tarafdar, P. K.; Swamy, M. J. *J. Lipid Res.* **2010**, *51*, 42−52.
(26) Reddy, S. T.; Tarafdar, P. K.; Kamlekar, R. K.; Swamy, M. J. *J. Phys. Chem. B* **2013**, *117*, 8747−8757.
(27) Zhou, Q.-X.; Kohn, J. *Macromolecules* **1990**, *23*, 3399−3406.
(28) Ramakrishnan, M.; Sheeba, V.; Komath, S. S.; Swamy, M. J. *Biochim. Biophys. Acta* **1997**, *1329*, 302−310.
(29) Marsh, D. *Handbook of Lipid Bilayers*; CRC Press: Boca Raton, FL., 1990; pp 387.
(30) Sheldrick, G. M. *Acta Crystallogr.* **2008**, *A64*, 112−122.
(31) Tarafdar, P. K.; Reddy, S. T.; Swamy, M. J. *J. Phys. Chem. B* **2013**, *117*, 9900−9909.
(32) Tarafdar, P. K.; Reddy, S. T.; Swamy, M. J. *Cryst. Growth Des.* **2012**, *12*, 1132−1140.
(33) Ramakrishnan, M.; Swamy, M. J. *Biochim. Biophys. Acta* **1999**, *1418*, 261−267.
(34) Kamlekar, R. K.; Swamy, M. J. *J. Lipid Res.* **2006**, *47*, 1424−1433.
(35) Dahlén, B.; Pascher, I.; Sundell, S. *Acta Chem. Scand. A* **1977**, *31*, 313−320.
(36) Marsh, D.; Swamy, M. J. *Chem. Phys. Lipids* **2000**, *105*, 43−69.
(37) Head-Gordon, T. *Proc. Natl. Acad. Sci. U.S.A.* **1995**, *92*, 8308−8312.
(38) Marsh, D. In *Supramolecular Structure and Function. Biomembranes*; Pifat, G., Herak, J. N., Eds.; Plenum Press: New York, 1982; pp 127−178.
(39) Hou, X.; Schober, M.; Chu, Q. *Cryst. Growth Des.* **2012**, *12*, 5159−5163.
(40) Alkorta, I.; Rozas, I.; Elguero, J. *Chem. Soc. Rev.* **1998**, *27*, 163−170.
(41) Desiraju, G. R. *Acc. Chem. Res.* **1996**, *29*, 441−449.
(42) Blatchford, M. A.; Raveendran, P.; Wallen, S. L. *J. Am. Chem. Soc.* **2000**, *124*, 14818−14819.
(43) Chang, H.-C.; Jiang, J.-C.; Chuang, C.-W.; Lin, S. H. *Chem. Phys. Lett.* **2004**, *397*, 205−210.
(44) Morris, D. G.; Ryder, K. S.; Muir, K. W. *Cryst. Growth Des.* **2005**, *5*, 361−364.
(45) Larsson, K. *Acta Crystallogr.* **1966**, *21*, 267−272.
(46) Goto, M.; Takiguchi, T. *Bull. Chem. Soc. Jpn.* **1985**, *58*, 1319−1320.
(47) Goto, M.; Kozawa, K.; Uchida, T. *Bull. Chem. Soc. Jpn.* **1988**, *61*, 1434−1436.
(48) Pascher, I.; Lundmark, M.; Nyholm, P.; Sundell, S. *Biochim. Biophys. Acta* **1992**, *1113*, 339−372.
(49) Pascher, I.; Sundell, S.; Hauser, H. *J. Mol. Biol.* **1981**, *153*, 807−824.
(50) Pascher, I.; Sundell, S. *Chem. Phys. Lipids* **1985**, *37*, 241−250.